# Ethanolysis of enzymatic hydrolysis lignin with Ni catalysts on different supports: the roles of catalytic sites

Yushuai Sang, ingze Yang, Hong Chen, Yongdan Li


PII: S0920-5861(24)00244-X

DOI: https://doi.org/10.1016/j.cattod.2024.114750

Reference: CATTOD114750

To appear in: *Catalysis Today*

Received date: 1 January 2024
Revised date: 6 April 2024
Accepted date: 21 April 2024

Please cite this article as: Yushuai Sang, ingze Yang, Hong Chen and Yongdan Li, Ethanolysis of enzymatic hydrolysis lignin with Ni catalysts on different supports: the roles of catalytic sites, *Catalysis Today,* (2024) doi:https://doi.org/10.1016/j.cattod.2024.114750

# Ethanolysis of enzymatic hydrolysis lignin with Ni catalysts on different supports: the roles of catalytic sites

Yushuai Sang,[b,c] ingze Yang,[b] Hong Chen*[a] and Yongdan Li*[b,c]

[a] *School of Environmental Science and Engineering, Tianjin University, Tianjin 300072, China*

[b] *Department of Chemical and Metallurgical Engineering, School of Chemical Engineering, Aalto University, Kemistintie 1, Espoo, P.O. Box 16100, FI-00076, Finland*

[c] *Collaborative Innovation Center of Chemical Science and Engineering (Tianjin), Tianjin Key Laboratory of Applied Catalysis Science and Technology, State Key Laboratory of Chemical Engineering (Tianjin University), School of Chemical Engineering and Technology, Tianjin University, Tianjin 300072, China*



**Abstract:** Catalytic lignin solvolysis (CLS) holds promise for efficient lignin utilization, yielding small molecules with minimal or no char formation. However, the role of different active sites of catalyst in CLS are rarely discussed. Here, Ni catalysts on different supports, i.e., $SiO_2$, $Al_2O_3$, MgO, and $ZrO_2$, were prepared with the aim of manipulating the relative importance of metal and acid-base functionalities to investigate the role of different active sites in the enzymatic hydrolysis of lignin (EHL)

* Corresponding author. E-mail address: chenhong_0405@tju.edu.cn (H. Chen).
* Corresponding author. E-mail: yongdan.li@aalto.fi (Y. Li)

ethanolysis. The main ether linkage, i.e., β-O-4, in EHL is cleaved without the participation of a catalyst. Metal sites suppress repolymerization through hydrogenating active intermediates, while acid and base sites facilitate the conversion of phenolic monomers into complex alkylated and etherified products and also promote repolymerization reactions. Among the catalysts, $Ni/SiO_2$ demonstrated the highest hydrogenation activity and yielded the most monomers (24.7 wt%) at 280 °C for 6 h under 2 MPa $H_2$ in ethanol. These findings shed light on the catalytic mechanisms in CLS, offering valuable insights for future catalyst design.

Graphical abstract

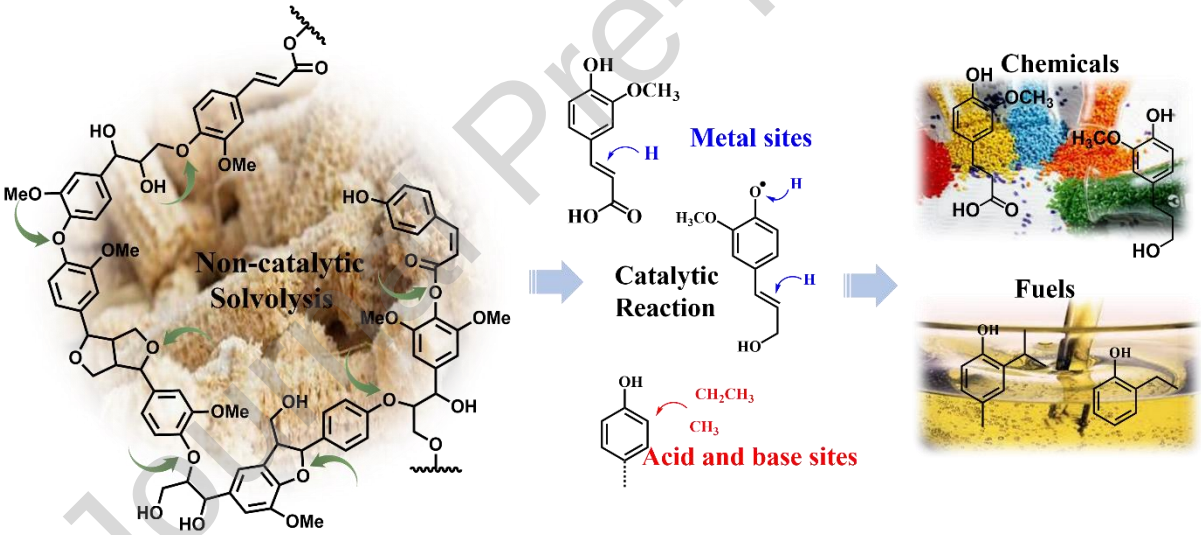


Keywords: Biomass, Lignin, Ethanolysis, Nickel catalyst, Reaction pathway

## 1. Introduction

Lignocellulose is the most abundant form of biomass, which mainly contains cellulose, hemicellulose and lignin [1]. As one of the important renewable resources, lignocellulose conversion into chemicals and fuels has been widely investigated.

Nowadays, second-generation (2G) biorefining technologies using agricultural and forestry residues have been developed for bioethanol production as a gasoline blend, with enzymatic hydrolysis lignin (EHL) as a large-scale by-product. To date, EHL has been burned for energy recovery and its efficient utilization technologies are in high demand. Lignin is a complex three-dimensional amorphous polymer, mainly consisting of three phenylpropanoid units: sinapyl, coniferyl and p-coumaryl alcohols [2]. As the only renewable resource containing rich aromatic units, lignin is an alternative feedstock to replace non-renewable petroleum to produce aromatic chemicals and fuels [3]. Meanwhile, efficient utilization of EHL to produce aromatic chemicals and fuels significantly improves the economy of the 2G biorefinery.

Catalytic solvolysis of lignin has received immense attention [3]. Some milestone works achieved complete lignin liquefaction and high monomer yields. Barta et al. [4] reported that $CuMgAlO_x$ was active in converting organosolv lignin into cyclohexyl derivatives in methanol at 300 ºC under an Ar atmosphere without the formation of char. Ma et al. [5] depolymerized Kraft lignin over an α-$MoC_{1-x}$/AC catalyst in ethanol at 280 ºC under $N_2$ atmosphere and achieved an overall yield of small-molecular chemicals, including esters, alcohols, arenes, phenols, and benzyl alcohols, was as high as 1.64 g/lignin. Huang et al. [6-8] depolymerized alkali lignin with $CuMgAlO_x$ catalyst in ethanol and obtained 60 wt% of alkylated mono-aromatics at 380 ºC under Ar atmosphere. Recently, we examined EHL solvolysis in ethanol and methanol with various catalysts, including $WO_3/Al_2O_3$ [9], $NiMo/Al_2O_3$ [10], unsupported Ni [11, 12] and $MoS_2$ [13, 14], and obtained high yields of alkylphenols (200-300 mg/g EHL)

without char formation. Compared to Mo and W-based catalysts, Ni catalysts typically yield higher monomer yields under relatively mild reaction conditions due to their higher hydrogenation activities [15]. Despite the widespread use of Ni catalysts supported on different metal oxides, such as $SiO_2$, $Al_2O_3$, MgO, and $ZrO_2$, in lignin solvolysis [16-19], the effect of catalyst support and the specific roles of different catalytic sites in lignin solvolysis have yet to be elucidated.

Herein, Ni catalysts on different supports, i.e., $SiO_2$, $Al_2O_3$, MgO, and $ZrO_2$, were prepared with the aim of manipulating the relative importance of metal and acid-base functionalities. Through comprehensive catalyst characterization and product analysis, the impact of catalyst support on enzymatic hydrolysis lignin (EHL) solvolysis was explored. With monitoring the cleavage of linkages in EHL using HSQC-NMR analysis, along with analyzing phenol conversion and adsorption over these catalysts, the process of EHL ethanolysis and the role of different catalytic sites are discussed.

## 2. Materials and methods

### 2.1. Materials

The EHL, a byproduct of the enzymatic hydrolysis of corncob, was provided by Shandong Longlive Co., and has a composition of 91.2 wt% lignin, 0.12 wt% residual carbohydrate and 1.42 wt% ash [10]. Ethanol and phenol of AR reagent grade were purchased from Guangfu Inc. $Ni(NO_3)_2 \cdot 6H_2O$, $SiO_2$, $Al_2O_3$, MgO and $ZrO_2$ were purchased from Aladdin Co., Ltd.

### 2.2. Methods

2.2.1 Reaction conditions

The EHL ethanolysis and phenol conversion were carried out in a 300 mL batch reactor (Parr 4566, made of Hastelloy) equipped with a temperature controller (Parr 4848) and a pressure sensor. Typically, 1.0 g of EHL or phenol and 60 mL of ethanol without catalyst or with 0.5 g catalyst were loaded into the reactor. The reactor was purged with 0 MPa $N_2$ for a non-catalytic reaction, and pressurized to 2 MPa $H_2$ for a catalytic reaction. The reactor was then heated to the prescribed temperature and kept for the prescribed time with stirring at 600 rpm. After the reaction, the product was filtrated to separate solid residue and liquid products.

2.2.2. Product analysis

The liquid product obtained in EHL ethanolysis and phenol conversion reactions were injected neatly into an Agilent 6890-5973 GC-MS for qualitative analysis. The monomer products were further analyzed quantitatively with an Agilent 6890 GC equipped with an FID. The working conditions for both GCs were the same as our previous works [11, 12]. Anisole was used as the internal standard to quantify the products. The total monomer yield was calculated with equation (1):

$$\text{Total monomer yield (wt\%)} = \frac{\text{The weight of total monomers}}{\text{The weight of EHL put into the reactor}} \times 100\% \quad (1)$$

When using phenol, the conversion of reactants and yield of products were calculated based on equations (2) and (3), respectively.

$$\text{Reactant conversion (mol\%)} = \frac{\text{n(reactant)}_{\text{initial}} - \text{n(reactant)}_{\text{residual}}}{\text{n(reactant)}_{\text{initial}}} \times 100\% \quad (2)$$

$$\text{Product yield(mol\%)} = \frac{\text{n(product)}}{\text{n(reactant)}_{\text{initial}}} \times 100\% \quad (3)$$

Where "n" represents the mole number.

Heteronuclear single quantum coherence-nuclear magnetic resonance (HSQC-NMR) spectra were recorded on a Bruker AVANCE III HD 400 MHz. 40 mg liquid product after the removal of ethanol was dissolved in DMSO-$d_6$ (0.5 mL as the deuterated NMR solvent). The molecular weights of large molecules produced from phenol conversion were measured with a matrix-assisted laser desorption/ionization time-of-flight mass spectrometry (MALDI-TOF-MS) with an Autoflex tof/toflll equipment made by American Bruker Dalton Corporation. A 15 g/L solution of 2, 5-dihydroxyl benzoic acid (DHB) (Sigma) in ethanol was used as a matrix.

The solid residue obtained from EHL ethanolysis was washed with 60 mL of ethanol, and then dried at 100 ºC for 12 h. The mass was measured with an analytical balance. The yield of char was calculated using equation (4):

$$\text{Char yield} = \frac{\text{The weight of solid residue} - \text{The weight of the catalyst}}{\text{The weight of EHL put into the reactor}} \times 100\% \qquad (4)$$

2.2.3. Phenol adsorption on a catalyst

0.1 g of catalyst was put into 10 mL phenol/cyclohexane solution (1:9, v:v). After 12 h, the catalyst was separated from the solution by centrifugation, and then washed with 20 mL pure cyclohexane for six times. The FTIR spectra of adsorbed phenol were collected with a Fourier transform infrared spectrometer (Thermo Fisher, Nicolet IS50) equipped with an MCT narrowband detector. The scan number was 256 and the spectral resolution was set as 4 $cm^{-1}$.

2.2.4. Catalyst preparation and characterization

All the catalyst samples were prepared through an incipient wetness impregnation technique with prescribed 10 wt% Ni loading. The sample was dried at 100 ºC for 12

h, and then calcined at 450 ºC for 4 h in air. The reduction was carried out in flowing $H_2$ (100 mL/min, STP) at 450 ºC for 4 h with a heating rate of 10 ºC /min.

X-ray diffraction (XRD) patterns were obtained with a Rigaku D/max 2500 v/pc instrument (Rigaku Corp. Japan) with Cu Kα radiation at a scanning rate of 5 º/$min^{-1}$. The Ni content of the samples was determined with an inductive coupled plasma-optical emission spectroscope (ICP-OES, VISTA-MPX, Varian). $H_2$ chemisorption was determined with a Micromeritics AutoChem 2920 instrument equipped with a quartz U-tube reactor and a thermal conductivity detector. $H_2$ temperature-programmed reduction ($H_2$-TPR) was carried out on TPDRO (TP-5080, Xianquan Co.) with a thermal conductivity detector (TCD). $NH_3$ and $CO_2$ temperature programmed desorption ($NH_3$-TPD and $CO_2$-TPD) were carried out in a fixed bed reactor using a gas mass spectrometer (HPR20, Hiden) as the detector. Brunauer-Emmett-Teller (BET) surface area of the samples was measured with a Micromeritics ASAP2020M system. Raman spectrometer (Renishaw inVia) with a 633 nm He-Ne laser excitation source was used for Raman analysis. X-ray photoelectron spectra (XPS) were recorded with an ESCALAB 250 Xi XPS spectrometer equipped with an Al-Kα ($h\nu$ = 1486.6 eV)

## 3. Results

### 3.1. EHL ethanolysis

The gas chromatogram of products and structure of monomers obtained from EHL ethanolysis are shown in Figure 1. Without a catalyst, phenols without alky sidechain (1 and 3) and para-ethyl phenols (5 and 7) are the main products, while esters derived from p-coumaric and ferulic acids (12, 13 and 14), as well as ortho-ethyl and ethyl

etherified products (4, 8 and 9), are also detected. With Ni/MgO as the catalyst, the product becomes more complex. Although phenols without side chains (1 and 3) and para-alkyl phenols (2, 5-7) are also detected, ortho-alkylated and etherified products (4, 8, 9, 15-24) become the main products. Alkylated products (17, 18, 22, 23, and 26) with isopropyl and tert-butyl side chains are also measured. In addition, the phenolic hydroxyls of esters (25 and 14) are also etherified. The molecules obtained with $Ni/Al_2O_2$ are similar to those obtained with Ni/MgO, but two tert-butyl substituted molecules (22 and 23) disappear and a double isopropyl substituted molecule (27) appears. In the case of $Ni/ZrO_2$, comparatively small amounts of ortho-alkylated and etherified molecules (8 and 27) are detected, and most of the monomers are para-alkyl phenols (2, 5-7, 10, 11, 28) and esters (12 and 13). In addition, para-propanol substituted phenol (31) appears. In $Ni/SiO_2$ catalyzed reaction, no ortho-alkylated and etherified molecules are detected. Compared to $Ni/ZrO_2$, $Ni/SiO_2$ produced larger amounts of esters (12 and 13) and para-propanol substituted phenol (31), but lower amounts of para-ethyl phenols (5 and 7). The formation of 12, 13 and 31 is attributed to the effective hydrogenation of C=C double bonds in the side chains of primary monomers, effectively suppressing their decomposition reactions [11, 12]. The higher amounts of these compounds obtained with $Ni/SiO_2$ compared to $Ni/ZrO_2$ suggest that $Ni/SiO_2$ exhibits superior hydrogenation activity compared to $Ni/ZrO_2$.

The monomers obtained from EHL depolymerization are classified into two types (Figure 2(a)): Ortho-alkylated and etherified products are derived from alkylation and etherification reactions, and are sorted as **Os**. Phenols without side chains, para-alkyl

phenols, aromatic esters, and propanol-substituted phenols are derived from the primary lignin monomers, as revealed in our previous works [11, 12], and are sorted as **Ls**. The monomer and char yields obtained without and with different catalysts are given in Figure 2(b). Without a catalyst, 29.8 wt% char is formed, and 10.2 wt% total monomer yield is obtained, mainly including **Ls**. With the presence of a catalyst, the yield of char significantly decreases. The yields of char obtained with Ni/MgO and $Ni/Al_2O_3$ are 7.3 and 3.7 wt%, respectively, and no char was formed with $Ni/ZrO_2$ and $Ni/SiO_2$ as catalysts, indicating a complete EHL liquefaction. High yields of **Os** are produced with Ni/MgO and $Ni/Al_2O_3$ as catalysts, while $Ni/ZrO_2$ and $Ni/SiO_2$ nearly only produce **Ls**. The total monomer yields obtained with $Ni/ZrO_2$ and $Ni/SiO_2$ are also higher than those obtained with Ni/MgO and $Ni/Al_2O_3$, and the highest total monomer yield, i.e. 24.7wt%, is obtained with $Ni/SiO_2$.

The HSQC-NMR spectra are given in Figure 3 and the signals are assigned according to the literature [8, 20, 21]. In the spectrum of original EHL, strong signals of aryl ethers with β-O-4 linkage ($A_\alpha$, $A_\beta$, $A_\gamma$) are recognized. After the reaction without a catalyst, these signals completely disappear, indicating that the cleavage of β-O-4 linkage can be achieved without a catalyst. The addition of different catalysts do not affect the β-O-4 linkage cleavage but affects the intensity of the signals of phenolic products. High yields of alkylated and etherified phenols are produced in $Ni/Al_2O_3$ and Ni/MgO catalyzed reactions, and hence the intensive signals of the alkyl and alkoxy are observed in their spectra. $Ni/Al_2O_3$ and Ni/MgO also show high activities for demethylation or/and demethoxylation reactions, as the signal of methoxyl ($-OCH_3$) is

significantly weakened. With $Ni/ZrO_2$ and $Ni/SiO_2$ as the catalysts, the signal of $-OCH_3$ is strengthened, and the signal of alkyl is weakened, while the signal of alkoxy disappears. Additionally, stronger signals of phenolic esters are observed with $Ni/ZrO_2$ and $Ni/SiO_2$ catalysts compared to $Ni/Al_2O_3$ and Ni/MgO catalysts, consistent with the higher yields of phenolic esters produced in reactions catalyzed by $Ni/ZrO_2$ and $Ni/SiO_2$. However, the signal of phenolic esters is also observed in the spectrum obtained without a catalyst, although phenolic esters are not detected in the non-catalytic reaction. This may be due to the fact that phenolic esters with carbon-carbon double bonds readily undergo condensation reactions [15], forming larger molecules that cannot be detected by GC-MS.

### 3.4. Phenol conversion and adsorption

#### 3.4.1. Phenol conversion

Phenol conversion gives the comparative activities of the catalyst for hydrogenation and alkylation/etherification. The product yields and phenol conversions are shown in Figure 4(a). With Ni/MgO and $Ni/Al_2O_3$ as catalysts, etherified and alkylated phenols (APs) are the main products, with the yields of 36.9 and 34.0 mol%, respectively, and small amounts of benzene ring hydrogenated products (HPs) are also produced, with the yields of 6.7 and 15.3 mol%, respectively. Nevertheless, HPs are the main products for $Ni/ZrO_2$ and $Ni/SiO_2$. The yield of HPs obtained with $Ni/ZrO_2$ is 65.4 mol%, and increases to 86.8 mol% with $Ni/SiO_2$. The yield of APs obtained with $Ni/ZrO_2$ is 8.5 mol% and decreases to 2.1 mol% with $Ni/SiO_2$. Without a catalyst, only 5.3 mol% of APs are detected. The phenol conversions for Ni/MgO and $Ni/Al_2O_3$ are

54.5 and 63.7 mol%, respectively, lower than that of $Ni/ZrO_2$ and $Ni/SiO_2$, which are 82.8 and 91.2 mol%, respectively. For the reaction without a catalyst, the phenol conversion is only 6.7 mol %. The results indicate that $Ni/SiO_2$ has the highest hydrogenation activity among the catalyst samples, while Ni/MgO and $Ni/Al_2O_3$ have high activities for alkylation and etherification reactions.

The MALDI-TOF-MS is used to analyze the large molecules formed in phenol conversion, and the results are presented in Figure 4 (b). During the non-catalytic phenol conversion, strong peaks of large molecules appear in the range of 250-300 m/z, together with several weak peaks in the range of 300-400 m/z. When Ni/MgO and $Ni/Al_2O_3$ are used as catalysts, strong peaks at above 400 m/z appear, indicating the formation of large molecules. In the cases with $Ni/ZrO_2$ as a catalyst, the number of peaks obviously decreases, but several peaks still appear in the range of 250-350 m/z. With $Ni/SiO_2$, the peaks of large molecules at above 250 m/z disappear, indicating that $Ni/SiO_2$ efficiently suppresses the condensation reactions of phenol.

3.4.1. Phenol adsorption

Phenol adsorption on the surface of catalysts was studied by FTIR analysis to reveal the interaction between lignin monomer and catalyst. The FTIR spectra are depicted in Figure 5, and the bands are assigned according to the literature [22-26]. In the spectrum of phenol adsorbed on Ni/MgO, the bands related to phenolic O-H (1475-1450 $cm^{-1}$, 1380-1360 $cm^{-1}$) disappear, and a band of C-O in phenolate species (1300-1230 $cm^{-1}$) is detected. Similar to Ni/MgO, bands of C-O in phenolate species are recorded and the bands related to phenolic O-H disappear, in the spectrum of phenol

adsorbed on Ni/$Al_2O_3$. In the case of Ni/$ZrO_2$, both the bands of phenolate species and phenolic O-H appear, indicating incomplete phenol dissociation over Ni/$ZrO_2$. In the spectrum of phenol adsorbed on Ni/$SiO_2$, the bands related to phenolic O-H are observed, and the bands of C-O in phenolate species are almost invisible, indicating non-dissociative over Ni/$SiO_2$.

3.5. Catalyst characterization

The $NH_3$-TPD profiles of catalyst supports are shown in Figure 6 (a). $Al_2O_3$ shows two desorption peaks centered at 180 and 410 ºC, which are ascribed to the desorption of $NH_3$ from weak and strong acid sites, respectively. For MgO, the desorption peak ascribed to weak acid sites is also centered at around 180 ºC, but the other desorption peak shifts to 320 ºC, which is ascribed to medium acid sites. The desorption peaks of $ZrO_2$ and $SiO_2$ are much lower than those of other supports, but still two peaks are visible in their curves. Meanwhile, the first desorption peaks of $ZrO_2$ and $SiO_2$ shift to lower temperatures, centered at 150 and 160 ºC, respectively, indicating that the strengths of weak acid sites on $ZrO_2$ and $SiO_2$ are weaker than those on $Al_2O_3$ and MgO. Nevertheless, the strengths of strong acid sites on $ZrO_2$ and $SiO_2$ are both similar to those on $Al_2O_3$, as their second peaks are also centered at around 400 ºC. The $CO_2$-TPD profiles of catalyst supports are shown in Figure 6 (b). MgO has two high desorption peaks centered at 240 and 500 ºC, which are ascribed to the desorption of $CO_2$ from weak and strong base sites, respectively. The strength of base sites of $Al_2O_3$ is slightly weaker than that of MgO, as the desorption peaks of $Al_2O_3$ are centered at 210 ºC and 430 ºC. The strengths of base sites of $ZrO_2$ is weaker than those of MgO and $Al_2O_3$,

with its desorption peaks centered at 150 and 330 ºC, respectively. Nevertheless, $SiO_2$ does not show desorption peaks of $CO_2$.

The total amounts of acidic/basic sites of different catalyst supports were calculared based on the areas of desorption peaks (Table 1). $Al_2O_3$ has the highest amounts of acidic sites and MgO has the highest amounts of basic sites among the samples, which are 29.5 μmol $NH_3$/g and 42.3 μmol $CO_2$/g, respectively. Meanwhile, $Al_2O_3$ contains small amounts of basic sites (8.7μmol $CO_2$/g) and MgO contains small amounts of acidic sites (7.7 μmol $NH_3$/g). Small amounts of acidic (4.2 μmol $NH_3$/g) and basic sites (3.6 μmol $NH_3$/g) exist on $ZrO_2$. $SiO_2$ has trace amounts of acidic sites (1.5 μmol $NH_3$/g) and contains no basic sites. The BET surface areas of these catalyst supports are also listed in Table 1. The BET surface areas of MgO and $Al_2O_3$ are 173.3 and 209.6 $m^2$/g, respectively. $ZrO_2$ has the smallest BET surface area, which is 67.6 $m^2$/g, and $SiO_2$ has the largest BET surface area, which is 313.2 $m^2$/g.

The $H_2$-TPR curves of catalysts are plotted in Figure 6 (c). The reduction peaks below 400 ºC are ascribed to the reduction of easily reducible NiO to metallic Ni, and the peaks in the temperature range of 400-500 ºC are attributed to the reduction of NiO in weak interaction with supports, and the peaks above 500 ºC are related to the reduction of NiO in strong interaction with supports [27-31]. Ni/$SiO_2$ has two reduction peaks at 370 and 440 ºC, and Ni/$ZrO_2$ has one peak at 400 ºC, indicating the weak interaction between Ni and $SiO_2$ and $ZrO_2$ supports. Hence, $Ni^{2+}$ ions in Ni/$SiO_2$ and Ni/$ZrO_2$ can be easily reduced when the reduction temperature was set as 450 ºC. Nevertheless, NiO has strong interaction with $Al_2O_3$ and MgO supports, as the peaks

above 500 °C appear in the curves of $Ni/Al_2O_3$ and Ni/MgO. In particular, peaks at 770 and 760 °C in the curves of $Ni/Al_2O_3$ and Ni/MgO are ascribed to the reduction of $NiAl_2O_4$ and NiO-MgO solid solution, respectively [29, 30].

The XRD patterns of the catalyst samples after reduction in $H_2$ at 450 °C are shown in Figure 6 (d). The diffraction peaks of metallic Ni (PDF#65-2865) can be observed in the patterns of the reduced catalyst samples except for that of Ni/MgO in which only the diffraction peaks of MgO are visible. In the pattern of $Ni/Al_2O_3$, the diffraction peaks of $NiAl_2O_4$ are also observed, indicating that $NiAl_2O_4$ cannot be completely reduced under this condition. The ratio of metallic Ni ($Ni^0$) to ionic Ni ($Ni^{2+}$) on the catalyst surface is determined with XPS analysis (Figure 6 (e)). The ratio of $Ni^0$ and $Ni^{2+}$ on $Ni/SiO_2$ and $Ni/ZrO_2$ are 0.42 and 0.37, respectively, but these values on $Ni/Al_2O_3$ and Ni/MgO are only 0.18 and 0.10, respectively. This indicates that the reduction degree of Ni in $Ni/Al_2O_3$ and Ni/MgO is much lower than that in $Ni/SiO_2$ and $Ni/ZrO_2$.

The real Ni loadings and Ni dispersions of different catalysts are listed in Table 2. The real Ni loadings are close to the prescribed value of 10 %. Ni/MgO exhibits the highest Ni dispersion, i.e., 23.1% among the samples, due to the strong interaction between Ni and MgO. Following Ni/MgO, the Ni dispersion of $Ni/SiO_2$ and $Ni/Al_2O_3$ are 14.5% and 12.0 %, respectively. Nevertheless, $Ni/ZrO_2$ has the lowest Ni dispersion, i.e., 6.1 %, among these catalysts.

## 4. Discussion

4.1. Non-catalytic reaction

The HSQC-NMR results indicate that the cleavage of main ether linkages, i.e., β-O-4, occurs via homogeneous steps and does not need a catalyst. In the early works, non-catalytic ethanolysis of Kraft lignin was supposed to be induced with the radicals formed from ethanol homolysis [5, 32, 33]. However, the bond dissociation energies (BDEs) of β-O-4 ether linkages in lignin are lower (54-72 kcal/mol) than the BDEs of chemical bonds in ethanol (94-110 kcal/mol) [34, 35], indicating that ethanol decomposition into free radicals is more challenging than homolysis of ether linkages. In addition, only 1,1-diethoxyethane was detected as the product of ethanol self-conversion in the non-catalytic reaction. These observations suggest that the non-catalytic reaction should not follow a free radical reaction mechanism. Recently, Li et al. [36] reported that the homolysis of β-O-4 linkages in lignin model compound with phenolic hydroxyl end-units readily occur at around 200 ºC, but is difficult in the compounds with methoxy end-units. Here, we clarify the process of non-catalytic lignin depolymerization, and show it in Scheme 1. The reaction starts from the phenolic hydroxyl end-units which undergo a homolysis reaction first. The radical formed from homolysis snatch H from ethanol or $H_2$, forming new phenolic hydroxyl end-units, and then repeat homolysis reaction. Although EHL is efficiently depolymerized at 280 ºC in the non-catalytic reaction, achieving complete cleavage of β-O-4 linkages, radical-induced repolymerization reactions occur extensively in the absence of a catalyst [37], leading to the formation of a high yield of char.

4.2. The role of the catalytic sites

As $ZrO_2$ and $SiO_2$ have minimal acid/base sites, the activity of Ni/$ZrO_2$ and Ni/$SiO_2$ in EHL ethanolysis predominantly relies on the hydrogenation activity of Ni metal sites. Notably, Ni/$SiO_2$, with high BET specific surface area and moderate Ni and $SiO_2$ interaction, exhibits superior Ni dispersion compared to Ni/$ZrO_2$, thus showing higher hydrogenation activity. In Ni/$SiO_2$ and Ni/$ZrO_2$ catalyzed EHL ethanolysis, the absence of char formation indicates the effective suppression of repolymerization reactions through hydrogenation reaction. Ni/$SiO_2$ is more efficient than Ni/$ZrO_2$, yielding a higher monomer yield in EHL ethnaolysis owing to its higher hydrogenation activity. As reported, monomers and intermediates containing carbon-carbon and carbon-oxygen double bonds in their chains are prone to undergo repolymerization reactions, but can be stabilized through hydrogenation reactions [38-41]. In addition, the active hydrogen species generated from $H_2$ dissociation over metal sites act as radical scavengers, effectively impeding radical-induced repolymerization reactions [42].

Strong interactions between Ni and supports form in Ni/$Al_2O_3$ and Ni/MgO after calcination, which result in their low Ni reduction degree at a moderate temperature reduction. Compard to Ni/$SiO_2$ and Ni/$ZrO_2$, Ni/$Al_2O_3$ and Ni/MgO display lower hydrogenation activity, but, with higher amounts of acid/base sites, they exhibit higher activity for phenol alkylation and etherification, indicating that acid and base sites serve as active sites for these reactions. Phenol is strongly adsorbed on Ni/MgO and Ni/$Al_2O_3$, and dissociated into phenolate, which is supported to be the intermediate of phenol alkylation and etherification reactions [43-45]. In EHL ethanolysis reactions, Ni/MgO and Ni/$Al_2O_3$ catalysts also promote demethylation or/and demethoxylation reaction of

monomers, as revealed with HSQC-NMR analysis, and methyl and methoxy may also involve into alkylation and etherification reaction, forming complex **Os**. In the previous works, alkylation and etherification reactions are supposed to stabilize active phenolic monomers, hence suppressing repolymerization reactions [6, 7, 9, 10]. However, In $Ni/Al_2O_3$ and Ni/MgO catalyzed EHL ethanolysis reactions, inefficient suppression of repolymerization reactions leads to char formation. This indicate that alkylation and etherification reactions are less efficient than hydrogenation reaction in suppressing repolymerization reaction.

In Ni/MgO and $Ni/Al_2O_3$ catalyzed phenol conversion, we observed the formation of larger molecules compared to those generated in the non-catalytic reaction, indicating that acid and base sites also facilitate phenol polymerization. Phenol polymerization and phenol alkylation and etherification may proceed via the same intermediates, i.e., phenolates. Alkylation and etherification reactions can occur if phenolates react with alkoxy or alkyl groups, while repolymerization reactions may take place if two phenolates react with each other. In addition, larger molecules also cover the Ni metal sites, hindering the hydrogenation of intermediates.

4.2.3. Catalytic reaction

Early works proposed a two-step mechanism for catalytic lignin ethanolysis. Herein, the cleavage of lignin linkages and the role of different catalytic sites are further clarified. The reaction pathways of catalytic EHL ethanolysis are shown in Scheme 2. In the reaction, main ether linkages in EHL are cleaved via a non-catalytic reaction, and the intermediates are further converted over a catalyst. Metal sites dissociate $H_2$ into

active H which serves as radical scavengers, hindering the radical-induced coupling reactions [42]. In addition, carbon-carbon double bonds in p-coumaric and ferulic acids as well as coniferyl and sinapyl alcohols are hydrogenated over metal sites, preventing their decomposition reactions into alkenyl-phenols and phenols without sidechains [11, 12], and hence high yields of esters and para-propanol phenols are formed in $Ni/SiO_2$ catalyzed reaction. Acid and base sites promote the demethylation or/and demethoxylation reactions of lignin monomers, and methyl, methoxy, and ethanol further undergo alkylation and etherification with lignin monomers over acid and base sites, producing etherified and ortho-alkylated products [5, 46-50]. In addition, lignin monomers that are strongly adsorbed on the acid and base sites readily undergo condensation reactions.

## 4. Conclusion

Ni catalysts, including $Ni/SiO_2$, $Ni/Al_2O_3$, Ni/MgO, and $Ni/ZrO_2$, with different hydrogenation activity and acid/base functions are prepared and employed in EHL ethanolysis at 280 °C for 6 h under 2 MPa $H_2$. Ni/MgO and $Ni/Al_2O_3$ with high amounts of acid and base sites gave low total monomer yields but high yields of **Os**. $Ni/SiO_2$ with the highest hydrogenation activity achieves the highest yield of monomers of 24.7 wt%, among the catalysts examined.

The cleavage of main ether linkage, i.e., β-O-4, in EHL is achieved through a non-catalytic reaction, but the unstable monomers and intermediates formed undergo repolymerization steps. These unstable monomers and intermediates are stabilized through hydrogenation over the metal sites of the catalyst. The acid and base sites of

the catalyst not only promote alkylation and etherification reactions of monomers but also facilitate repolymerization steps.

## Acknowledgments

This work has received funding from the European Union's Horizon 2020 research and innovation program, (BUILDING A LOW-CARBON, CLIMATE RESILIENT FUTURE: SECURE, CLEAN AND EFFICIENT ENERGY) under Grant Agreement No 101 006 744. The content presented in this document represents the views of the authors, and the European Commission has no liability in respect of the content. The Tianjin colleagues thank the financial support from the National Natural Science Foundation of China under grant numbers: 21808163 and 21690083.

## Reference

[1] C. Li, X. Zhao, A. Wang, G.W. Huber, T. Zhang, Catalytic Transformation of Lignin for the Production of Chemicals and Fuels, Chem. Rev., 115 (2015) 11559-11624.

[2] A.J. Ragauskas, G.T. Beckham, M.J. Biddy, R. Chandra, F. Chen, M.F. Davis, B.H. Davison, R.A. Dixon, P. Gilna, M. Keller, P. Langan, A.K. Naskar, J.N. Saddler, T.J. Tschaplinski, G.A. Tuskan, C.E. Wyman, Lignin valorization: improving lignin processing in the biorefinery, Science, 344 (2014) 1246843.

[3] Z. Sun, B. Fridrich, A. de Santi, S. Elangovan, K. Barta, Bright Side of Lignin Depolymerization: Toward New Platform Chemicals, Chem. Rev., 118 (2018) 614-678.

[4] K. Barta, T.D. Matson, M.L. Fettig, S.L. Scott, A.V. Iretskii, P.C. Ford, Catalytic disassembly of an organosolv lignin via hydrogen transfer from supercritical methanol, Green Chem., 12 (2010) 1640-1647.

[5] R. Ma, W. Hao, X. Ma, Y. Tian, Y. Li, Catalytic Ethanolysis of Kraft Lignin into High-Value Small-Molecular Chemicals over a Nanostructured alpha-Molybdenum Carbide Catalyst, Angew. Chem., Int. Ed., 53 (2014) 7310-7315.

[6] X. Huang, T.I. Korányi, M.D. Boot, E.J.M. Hensen, Ethanol as capping agent and formaldehyde scavenger for efficient depolymerization of lignin to aromatics, Green Chem., 17 (2015) 4941-4950.

[7] X. Huang, T.I. Koranyi, M.D. Boot, E.J. Hensen, Catalytic depolymerization of lignin in supercritical

ethanol, ChemSusChem, 7 (2014) 2276-2288.
[8] X. Huang, C. Atay, T.I. Koranyi, M.D. Boot, E.J.M. Hensen, Role of Cu-Mg-Al Mixed Oxide Catalysts in Lignin Depolymerization in Supercritical Ethanol, ACS Catal., 5 (2015) 7359-7370.
[9] F. Mai, Z. Wen, Y. Bai, Z. Ma, K. Cui, K. Wu, F. Yan, H. Chen, Y. Li, Selective Conversion of Enzymatic Hydrolysis Lignin into Alkylphenols in Supercritical Ethanol over a $WO_3/\gamma$-$Al_2O_3$ Catalyst, Ind. Eng. Chem. Res., 58 (2019) 10255-10263.
[10] Y. Bai, K. Cui, Y. Sang, K. Wu, F. Yan, F. Mai, Z. Ma, Z. Wen, H. Chen, M. Chen, Y. Li, Catalytic Depolymerization of a Lignin-Rich Corncob Residue into Aromatics in Supercritical Ethanol over an Alumina-Supported NiMo Alloy Catalyst, Energy Fuels, 33 (2019) 8657-8665.
[11] Y. Sang, M. Chen, F. Yan, K. Wu, Y. Bai, Q. Liu, H. Chen, Y. Li, Catalytic depolymerization of enzymatic hydrolysis lignin into monomers over an unsupported nickel catalyst in supercritical ethanol, Ind. Eng. Chem. Res., 59 (2020) 7466-7474.
[12] Y. Sang, K. Wu, Q. Liu, Y. Bai, H. Chen, Y. Li, Catalytic Ethanolysis of Enzymatic Hydrolysis Lignin over an Unsupported Nickel Catalyst: The Effect of Reaction Conditions, Energy Fuels, 35 ( 2021) 519–528.
[13] Y. Ma, Y. Sang, K. Wu, Q. Liu, H. Chen, Y. Li, Selective production of 2-(tert-butyl)-3-methylphenol from depolymerization of enzymatic hydrolysis lignin with $MoS_2$ catalyst, Catal. Today, 408 (2023) 194-203.
[14] K. Wu, Y. Sang, S. Kasipandi, Y. Ma, H. Jiao, Q. Liu, H. Chen, Y. Li, Catalytic roles of Mo-based sites on $MoS_2$ for ethanolysis of enzymatic hydrolysis lignin into aromatic monomers, Catal. Today, 408 (2023) 211-222.
[15] Y. Sang, H. Chen, M. Khalifeh, Y. Li, Catalysis and chemistry of lignin depolymerization in alcohol solvents-A review, Catalysis Today, 408 (2023) 168-181.
[16] R. Shu, Y. Xu, P. Chen, L. Ma, Q. Zhang, L. Zhou, C. Wang, Mild hydrogenation of lignin depolymerization products over $Ni/SiO_2$ catalyst, Energy & fuels, 31 (2017) 7208-7213.
[17] S. Van den Bosch, T. Renders, S. Kennis, S.-F. Koelewijn, G. Van den Bossche, T. Vangeel, A. Deneyer, D. Depuydt, C. Courtin, J. Thevelein, Integrating lignin valorization and bio-ethanol production: on the role of Ni-Al 2 O 3 catalyst pellets during lignin-first fractionation, Green Chem., 19 (2017) 3313-3326.
[18] X. Chen, W. Guan, C.-W. Tsang, H. Hu, C. Liang, Lignin valorizations with Ni catalysts for renewable chemicals and fuels productions, Catalysts, 9 (2019) 488.
[19] F. Shu, G. Long, Y. Chen, Y. Gao, M. Jiang, J. Long, Boosting catalytic activity of $Ni/ZrO_2$ by introducing MoO3 on selective hydrogenolysis of lignin, Chem. Eng. Sci., (2024) 120036.
[20] S. Van den Bosch, W. Schutyser, R. Vanholme, T. Driessen, S.F. Koelewijn, T. Renders, B. De Meester, W.J.J. Huijgen, W. Dehaen, C.M. Courtin, B. Lagrain, W. Boerjan, B.F. Sels, Reductive lignocellulose fractionation into soluble lignin-derived phenolic monomers and dimers and processable carbohydrate pulps, Energy Environ. Sci., 8 (2015) 1748-1763.
[21] J.-L. Wen, S.-L. Sun, B.-L. Xue, R.-C. Sun, Recent Advances in Characterization of Lignin Polymer by Solution-State Nuclear Magnetic Resonance (NMR) Methodology, Materials, 6 (2013) 359-391.
[22] W.-C. Wu, L.-F. Liao, C.-F. Lien, J.-L. Lin, FTIR study of adsorption, thermal reactions and photochemistry of benzene on powdered $TiO_2$, Phys. Chem. Chem. Phys., 3 (2001) 4456-4461.
[23] J. Lichtenberger, S. Hargroveleak, M. Amiridis, In situ FTIR study of the adsorption and reaction of 2′-hydroxyacetophenone and benzaldehyde on MgO, J. Catal., 238 (2006) 165-176.
[24] F. Cavani, L. Maselli, S. Passeri, J.A. Lercher, Catalytic methylation of phenol on MgO - Surface

chemistry and mechanism, J. Catal., 269 (2010) 340-350.
[25] A. Popov, E. Kondratieva, J.-P. Gilson, L. Mariey, A. Travert, F. Maugé, IR study of the interaction of phenol with oxides and sulfided CoMo catalysts for bio-fuel hydrodeoxygenation, Catal. Today, 172 (2011) 132-135.
[26] L. Mino, A. Zecchina, G. Martra, A.M. Rossi, G. Spoto, A surface science approach to $TiO_2$ P25 photocatalysis: An in situ FTIR study of phenol photodegradation at controlled water coverages from sub-monolayer to multilayer, Appl. Catal. B, 196 (2016) 135-141.
[27] X. Zhang, W. Tang, Q. Zhang, T. Wang, L. Ma, Hydrocarbons production from lignin-derived phenolic compounds over $Ni/SiO_2$ catalyst, Energy Procedia, 105 (2017) 518-523.
[28] A. Morales-Marin, J.L. Ayastuy, U. Iriarte-Velasco, M.A. Gutierrez-Ortiz, E. Chemical Technologies, Nickel aluminate spinel-derived catalysts for the aqueous phase reforming of glycerol: Effect of reduction temperature, Appl. Catal. B-Environ., 244 (2019) 931-945.
[29] W.-w. Tang, X.-h. Zhang, Q. Zhang, T.-j. Wang, L.-l. Ma, Hydrodeoxygenation of Anisole over Ni/alpha-Al2O3 Catalyst, Chinese J. Chem. Phys., 29 (2016) 617-622.
[30] Q. Xiao, J. Xu, J. Zhang, Y. Sun, Y. Zhu, Exploring the morphological effect of $Ni_xMg_{1-x}O$ catalysts on CO2 reforming of methane, J. Energy Chem., 26 (2017) 325-329.
[31] M. Varkolu, V. Velpula, D.R. Burri, S.R.R. Kamaraju, Gas phase hydrogenation of levulinic acid to gamma-valerolactone over supported Ni catalysts with formic acid as hydrogen source, New J. Chem., 40 (2016) 3261-3267.
[32] X. Ma, R. Ma, W. Hao, M. Chen, F. Iran, K. Cui, Y. Tian, Y. Li, Common Pathways in Ethanolysis of Kraft Lignin to Platform Chemicals over Molybdenum-Based Catalysts, ACS Catal., 5 (2015) 4803-4813.
[33] F. Yan, R. Ma, X. Ma, K. Cui, K. Wu, M. Chen, Y. Li, Ethanolysis of Kraft lignin to platform chemicals on a $MoC_{1-x}/Cu\text{-}MgAlO_z$, catalyst, Appl. Catal. B-Environ., 202 (2017) 305-313.
[34] Y.M. Questell-Santiago, M.V. Galkin, K. Barta, J.S. Luterbacher, Stabilization strategies in biomass depolymerization using chemical functionalization, Nat. Rev. Chem., 4 (2020) 311-330.
[35] K. M. Bansal, Gordon R. Freeman, Free-radical chain reactions in the radiation-sensitized pyrolysis of ethanol vapor, J. Am. Chem. Soc., 90 (1968) 7190-7196.
[36] Y. Li, B. Demir, L.M. Vázquez Ramos, M. Chen, J.A. Dumesic, J. Ralph, Kinetic and mechanistic insights into hydrogenolysis of lignin to monomers in a continuous flow reactor, Green Chem., 21 (2019) 3561-3572.
[37] T. Kishimoto, Y. Sano, Delignification mechanism during high-boiling solvent pulping. Part 2. Homolysis of guaiacylglycerol-β-guaiacyl ether, Holzforschung, 56 (2002) 623-631.
[38] T. Renders, E. Cooreman, S. Van den Bosch, W. Schutyser, S.F. Koelewijn, T. Vangeel, A. Deneyer, G. Van den Bossche, C.M. Courtin, B.F. Sels, Catalytic lignocellulose biorefining in n-butanol/water: a one-pot approach toward phenolics, polyols, and cellulose, Green Chem., 20 (2018) 4607-4619.
[39] S. Van den Bosch, T. Renders, S. Kennis, S.F. Koelewijn, G. Van den Bossche, T. Vangeel, A. Deneyer, D. Depuydt, C.M. Courtin, J.M. Thevelein, W. Schutyser, B.F. Sels, Integrating lignin valorization and bio-ethanol production: on the role of $Ni\text{-}Al_2O_3$ catalyst pellets during lignin-first fractionation, Green Chem., 19 (2017) 3313-3326.
[40] C.W. Lahive, P.J. Deuss, C.S. Lancefield, Z. Sun, D.B. Cordes, C.M. Young, F. Tran, A.M. Slawin, J.G. de Vries, P.C. Kamer, N.J. Westwood, K. Barta, Advanced Model Compounds for Understanding Acid-Catalyzed Lignin Depolymerization: Identification of Renewable Aromatics and a Lignin-Derived Solvent, J. Am. Chem. Soc., 138 (2016) 8900-8911.

[41] P.J. Deuss, M. Scott, F. Tran, N.J. Westwood, J.G. de Vries, K. Barta, Aromatic monomers by in situ conversion of reactive intermediates in the acid-catalyzed depolymerization of lignin, J. Am. Chem. Soc., 137 (2015) 7456-7467.
[42] S. Chu, A.V. Subrahmanyam, G.W. Huber, The pyrolysis chemistry of a β-O-4 type oligomeric lignin model compound, Green chemistry, 15 (2013) 125-136.
[43] S. Sato, K. Koizumi, F. Nozaki, Ortho-selective methylation of phenol catalyzed by $CeO_2$-MgO prepared by citrate process, J. Catal., 178 (1998) 264-274.
[44] K. Tanabe, W.F. Hölderich, Industrial application of solid acid–base catalysts, Appl. Catal. A- Gen, 181 (1999) 399-434.
[45] K. Sreekumar, S. Sugunan, Ferrospinels based on Co and Ni prepared via a low temperature route as efficient catalysts for the selective synthesis of o-cresol and 2, 6-xylenol from phenol and methanol, J. Mol. Catal. A Chem., 185 (2002) 259-268.
[46] K. Cui, L. Yang, Z. Ma, F. Yan, K. Wu, Y. Sang, H. Chen, Y. Li, Selective conversion of guaiacol to substituted alkylphenols in supercritical ethanol over $MoO_3$, Appl. Catal. B-Environ., 219 (2017) 592-602.
[47] F. Mai, K. Cui, Z. Wen, K. Wu, F. Yan, M. Chen, H. Chen, Y. Li, Highly selective conversion of guaiacol to tert-butylphenols in supercritical ethanol over a $H_2WO_4$ catalyst, RSC Adv., 9 (2019) 2764-2771.
[48] F. Yan, Y. Sang, Y. Bai, K. Wu, K. Cui, Z. Wen, F. Mai, Z. Ma, L. Yu, H. Chen, Y. Li, Guaiacol demethoxylation catalyzed by $Re_2O_7$ in ethanol, Catal. Today, (2019).
[49] F. Yan, Z. Wen, K. Wu, K. Cui, F. Mai, Z. Ma, Y. Sang, Y. Bai, H. Chen, Y. Li, Deoxyalkylation of guaiacol using haggite structured V4O6(OH)(4), Catal. Sci. Technol., 9 (2019) 1922-1932.
[50] K. Wu, S. Kasipandi, Z. Wen, F. Yan, Y. Sang, Z. Ma, M. Chen, H. Chen, Y. Li, Selective demethoxylation of guaiacol to alkylphenols in supercritical methanol over a HT-$MoS_2$ catalyst, Catal. Today, (2020).

Table 1. Total acidic/basic sites and BET surface areas of different supports

| Catalyst | Total acidic sites (μmol $NH_3$/g) | Total basic sites (μmol $CO_2$/g) | BET surface area ($m^2$/g) |
|---|---|---|---|
| MgO | 7.7 | 42.3 | 173.3 |
| $Al_2O_3$ | 29.5 | 8.7 | 209.6 |
| $ZrO_2$ | 4.2 | 3.6 | 67.6 |
| $SiO_2$ | 1.5 | 0 | 313.2 |

Table 2. Ni loading and Ni dispersion of different Ni catalysts

| Catalyst | Ni loading (%) | Ni dispersion (%) |
|---|---|---|
| Ni/MgO | 10.7 | 23.1 |
| Ni/$Al_2O_3$ | 9.7 | 14.5 |
| Ni/$ZrO_2$ | 9.5 | 6.1 |

| | | |
|---|---|---|
| $Ni/SiO_2$ | 10.6 | 12.0 |

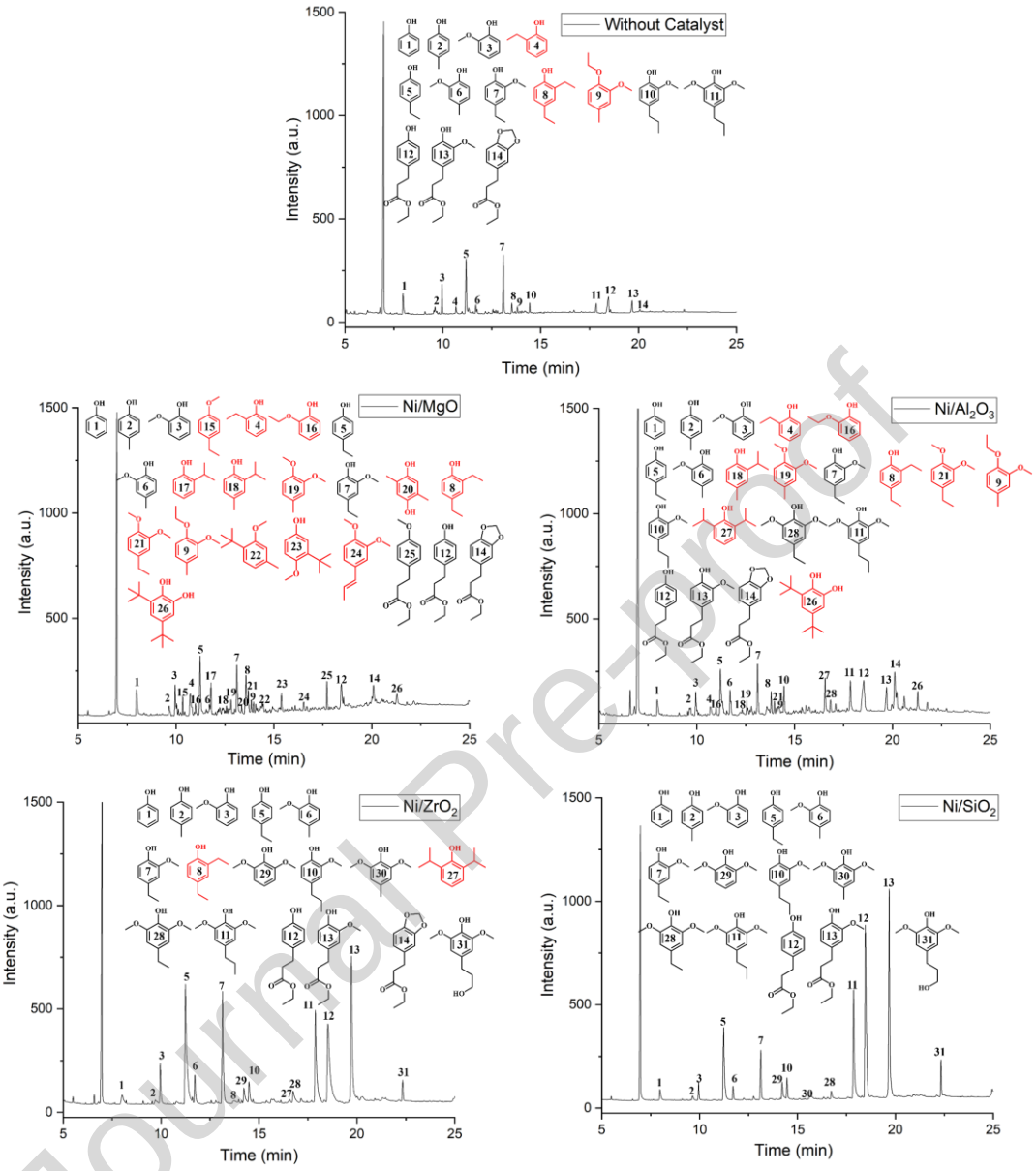


Figure 1. Gas chromatograms of products and structures of monomers obtained from EHL ethanolysis without catalyst and with the different Ni catalysts. (Reaction conditions: 1.0 g EHL, 0.5 g catalyst, 60 mL ethanol, 280 °C, 6 h, 2 MPa $H_2$)

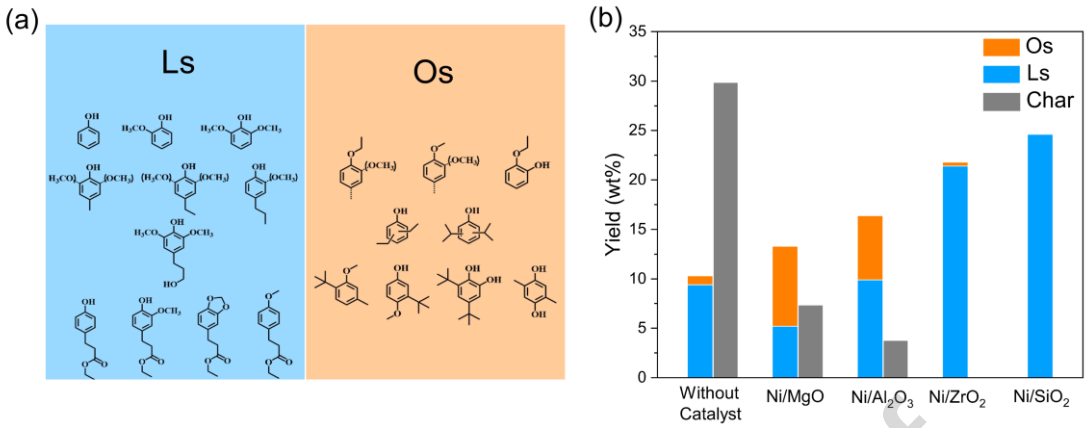


Figure 2. (a) classification of products obtained from EHL ethanolysis. (b) yields of char and monomers obtained from EHL ethanolysis without catalyst and with different Ni catalysts. (Reaction conditions: 1.0 g EHL, 0.5 g catalyst, 60 mL ethanol, 280 °C, 6 h, 2 MPa $H_2$)

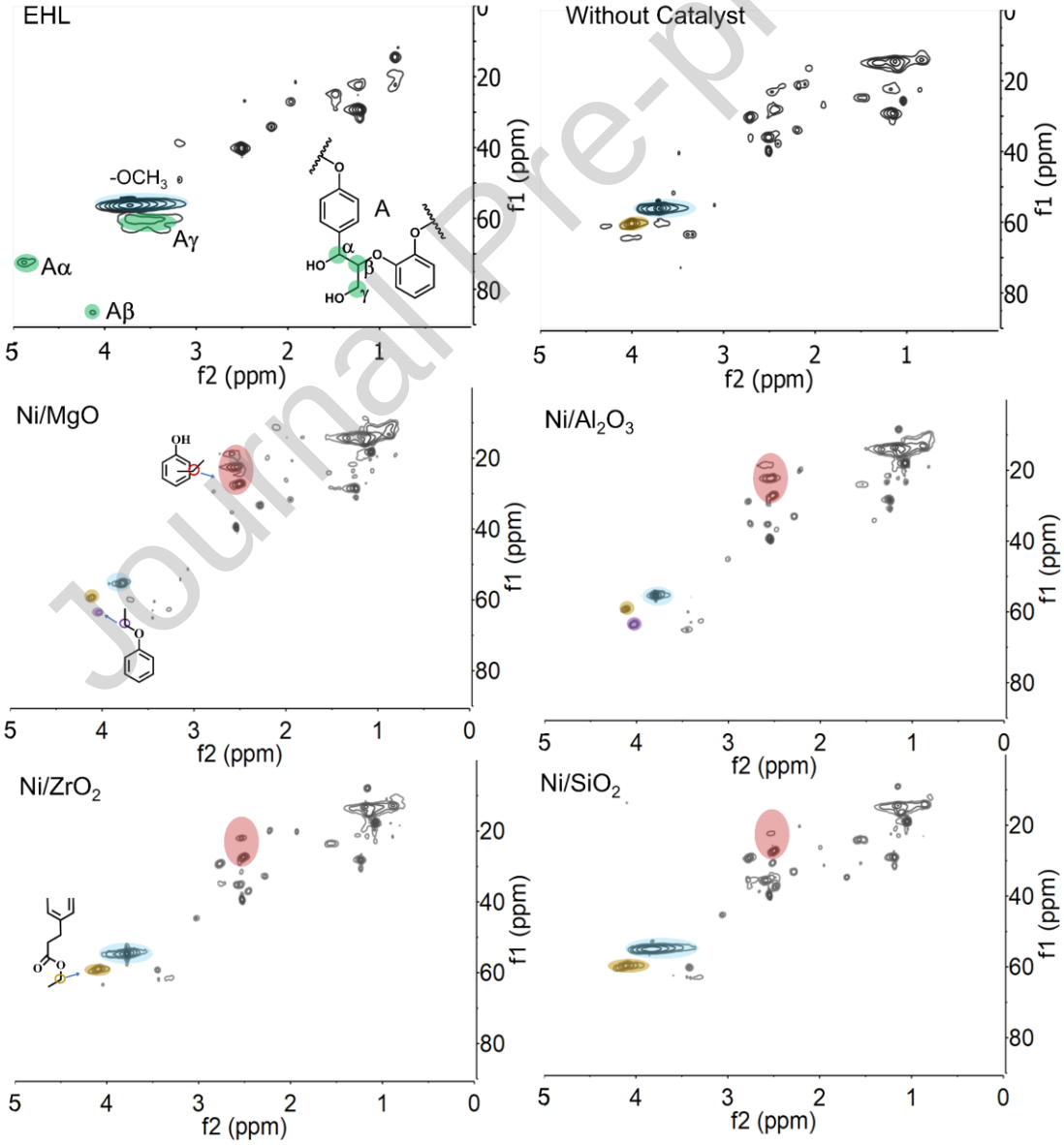

Figure 3. The HSQC NMR spectra of original EHL and liquid products obtained from EHL ethanolysis without catalyst and with the different Ni catalysts. (Reaction conditions: 1.0 g EHL, 0.5 g catalyst, 60 mL ethanol, 280 °C, 6 h, 2 MPa $H_2$)

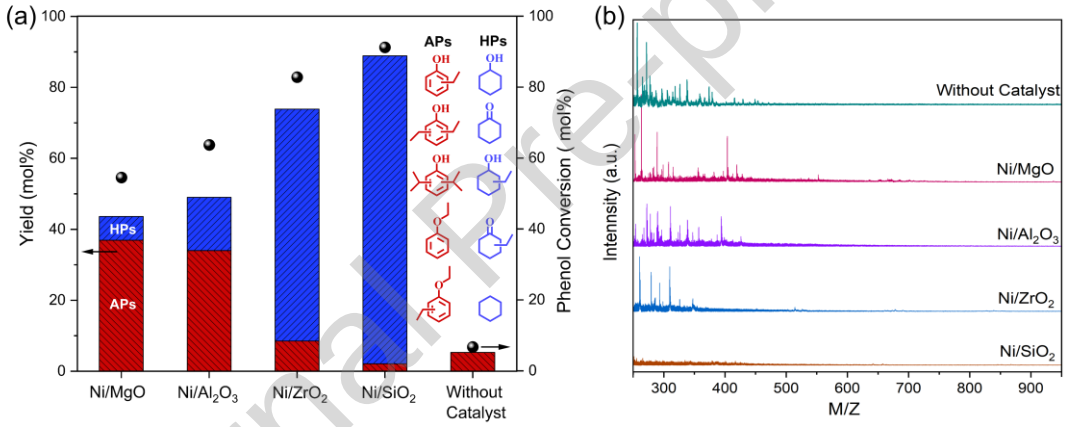


Figure 4. (a) the reactant conversion and product yield and (b) the MALDI-TOF-MS profiles of the products obtained from phenol conversion without catalyst and with the different Ni catalysts. (Reaction conditions: 1.0 g phenol, 0.5 g catalyst, 60 mL ethanol, 280 °C, 6 h, 2 MPa $H_2$)

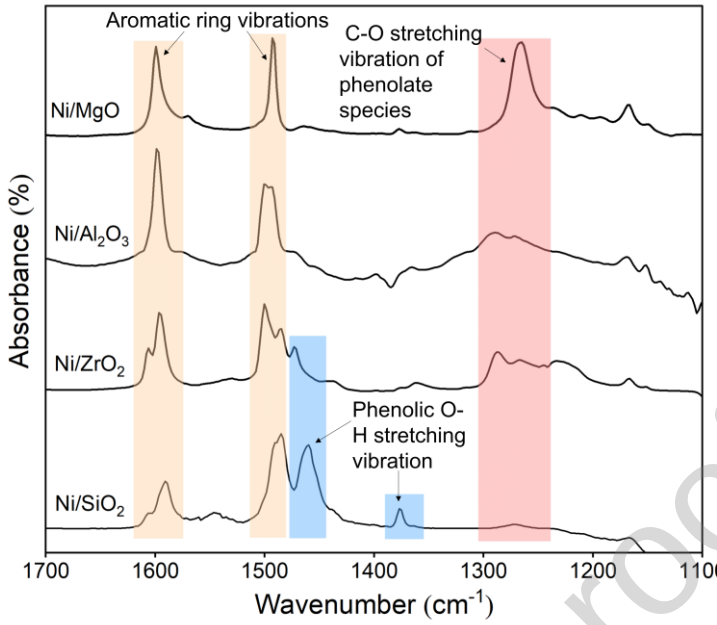


Figure 5. The FTIR spectrum of phenol adsorbed on different Ni catalysts

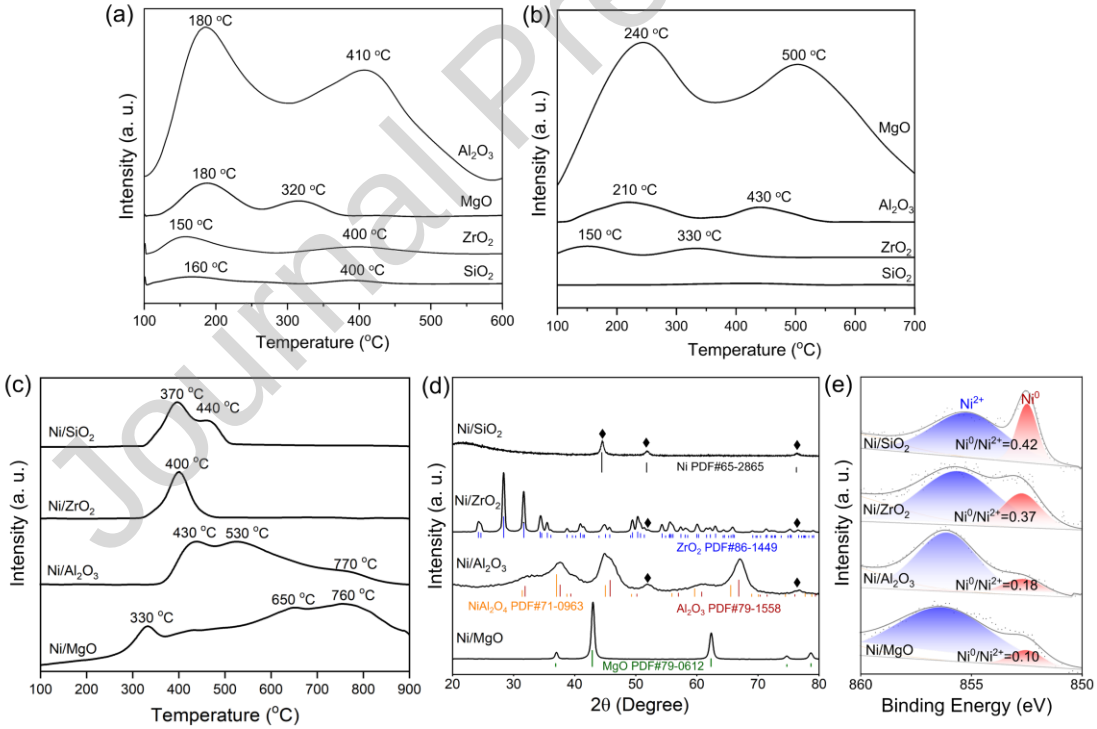


Figure 6. (a) $NH_3$-TPD and (b) $CO_2$-TPD profiles of different catalyst supports (c) $H_2$-TPR profiles of different catalysts and (d) XRD and (e) XPS of reduced catalysts

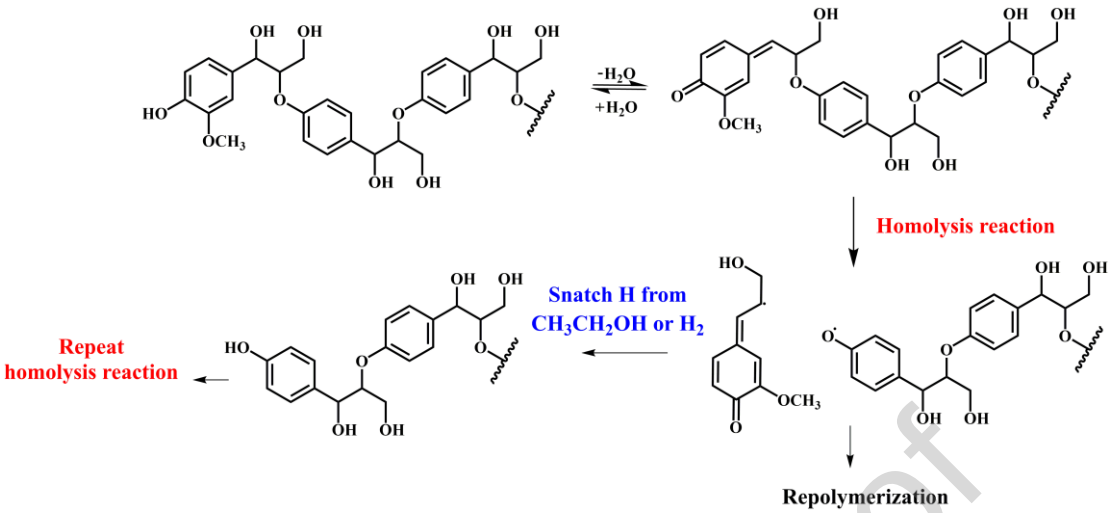


Scheme 1. The reaction pathways of non-catalytic EHL ethanolysis

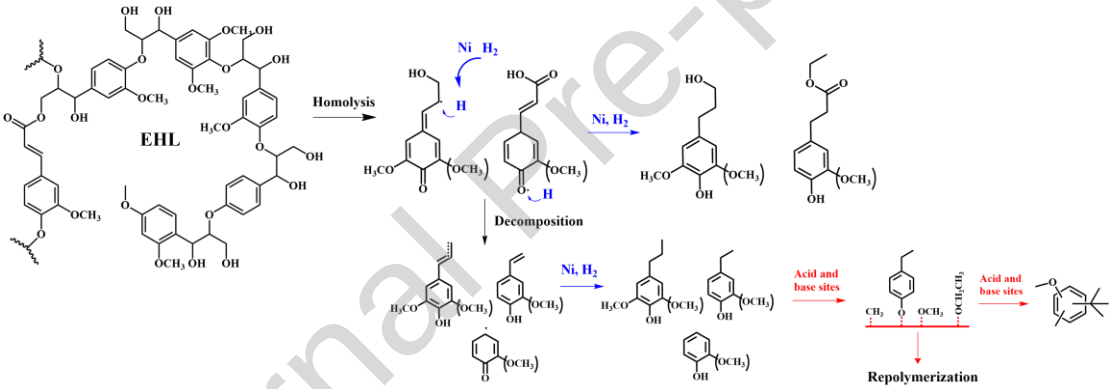


Scheme 2. The reaction pathways of catalytic EHL ethanolysis



## Declaration of interests

None

Highlights

1. EHL ethanolysis with Ni/$SiO_2$, Ni/$Al_2O_3$, Ni/MgO, and Ni/$ZrO_2$ were examined.
2. The role of metal sites and acid/base sites on EHL ethanolysis were investigated.
3. The β-O-4 in EHL is cleaved via homolysis reaction.
4. Metal sites suppress product repolymerization through hydrogenation reactions.
5. Acid/base sites promote alkylation, etherification and condensation reactions.